

On the Existence of Static Equilibria of a Cable-Suspended Load with Non-stopping Flying Carriers

Chiara Gabellieri* and Antonio Franchi*,[†]

Abstract— This work answers positively the question whether non-stop flights are possible for maintaining constant the pose of cable-suspended objects. Such a counterintuitive answer paves the way for a paradigm shift where energetically efficient fixed-wing flying carriers can replace the inefficient multirotor carriers that have been used so far in precise cooperative cable-suspended aerial manipulation. First, we show that one or two flying carriers alone cannot perform non-stop flights while maintaining a constant pose of the suspended object. Instead, we prove that *three* flying carriers can achieve this task provided that the orientation of the load at the equilibrium is such that the components of the cable forces that balance the external force (typically gravity) do not belong to the plane of the cable anchoring points on the load. Numerical tests are presented in support of the analytical results.

I. INTRODUCTION

Aerial robotic object manipulation has been largely studied also thanks to its interesting applications, e.g., transportation and assembly, to name a few [1]. Among the several manipulator designs proposed in the literature [2], simple lightweight and low-cost cables have attracted a lot of attention [3], especially due to the flying vehicle payload limitations.

Uncrewed helicopters have been used in [4] for transportation of suspended objects, while multirotor UAVs (Uncrewed Aerial Vehicles) have been typically considered [5], [6], [7], [8], [9], [10]. In the literature, we find examples of a slung load suspended below a single multi-rotor [11], [12] or a small helicopter [13]. Two multirotors have been widely exploited, especially for the manipulation of bar-shaped objects [14], [15], [16]. Three is the minimum number of robots to control the full pose of a cable-suspended rigid body object [17], and three multirotors have been studied, e.g., in [18], [5], [7], [19].

Compared to multirotor UAVs, fixed-wing UAVs have a longer flight endurance, as it has been shown, e.g., in [20]. However, fixed-wing UAVs cannot stop in mid-air, thus making seemingly impossible to keep the load in a static equilibrium while using such platforms as flying carriers. Furthermore, these platforms are unable to Vertical Take Off and Landing (VTOL). With an intermediate flight endurance,

* Robotics and Mechatronics Department, Electrical Engineering, Mathematics, and Computer Science (EEMCS) Faculty, University of Twente, 7500 AE Enschede, The Netherlands. c.gabellieri@utwente.nl, a.franchi@utwente.nl

[†] Department of Computer, Control and Management Engineering, Sapienza University of Rome, 00185 Rome, Italy, antonio.franchi@uniroma1.it

This work was partially funded by the Horizon Europe research and innovation programs under agreement no. 101059875 (Flyfic) and agreement no. 101120732 (Autoassess).

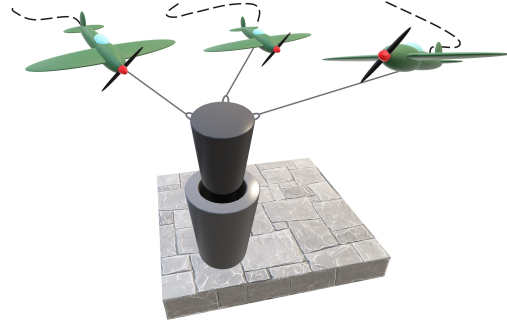


Fig. 1: Abstract representation of the concept whose theoretical feasibility is studied in this work. A team of non-stop flying carriers regulate the pose of a suspended object to a static forced equilibrium in an ideal application scenario.

convertible UAVs such as tail sitters have been proposed [20]. These are VTOL platforms that convert themselves to proceed flying as a fixed-wing platform. However, also these designs are obliged to follow non-stop trajectories to ensure an efficient flight.

Therefore, while non-stop UAVs may provide better endurance for cooperative cable suspended transportation tasks than multirotor UAVs, to the best of the authors' knowledge, it has not been systematically studied yet whether non-stop flights are compatible with keeping the load in a static equilibrium pose, i.e., whether it is possible to have at the same time the pose of the load being static while the flying carriers keep loitering above the object.

The theoretical discovery of such compatibility would pave the way to a completely new type of cable-suspended aerial systems, which would enable a much more energy-efficient execution of aerial manipulation tasks: long-distance transport would be combined with fine manipulation of the object's pose at the destination or in the presence of difficult intermediate passages, e.g., in cluttered environments. Figure 1 shows an abstract representation of the possible future scenario that would be enabled by this study.

In this work, we consider the challenges posed by the described intriguing problem and we study analytically whether there exist non-stop trajectories for the flying carriers that are compatible with the constraint of keeping the load at a constant static pose. We focus on the case in which the load must maintain a constant pose because it is obviously the most challenging case compared to the one in which also the load moves. The main contributions of the work are as follows: (i) we formalize the problem in mathematical terms;

(ii) we prove that with one and two carriers, non-stop flights are not achievable in the considered manipulation scenario; (iii) we prove that *three* is the minimum number of flying carriers for which non-stop flights are possible and (iv) we derive the conditions for that to hold, highlighting degenerate cases in which non-stop flights are prevented; (v) we support the theoretical results through numerical simulation.

The work is organized as follows. First, in Sec. II, we introduce the notation and the problem. Hence, we answer the above-described research question in Sec. III. In Sec. IV, we show numerical examples. Eventually, conclusions are drawn in Sec. V with an outline of future work.

II. PROBLEM STATEMENT

A. Mathematical background

Consider $\mathcal{F}_W = \{O_W, \mathbf{x}_W, \mathbf{y}_W, \mathbf{z}_W\}$, being a world-fixed frame where O_W is the origin, and $\mathbf{x}_W, \mathbf{y}_W, \mathbf{z}_W$ are the x-, y-, and z- axes, respectively. Similarly, consider a frame attached to the Center of Mass (CoM) of a rigid body, which represents the manipulated object, and denote it with $\mathcal{F}_B = \{O_B, \mathbf{x}_B, \mathbf{y}_B, \mathbf{z}_B\}$. The position of O_B in \mathcal{F}_W is denoted with $\mathbf{p}_L \in \mathbb{R}^3$ and $\mathbf{R}_L \in SO(3)$ expresses the attitude of \mathcal{F}_B w.r.t. \mathcal{F}_W . The body angular velocity expressed in the body frame is indicated as ${}^B\boldsymbol{\omega}_L$.

The rigid body is manipulated through n cables, each one of length $L_i > 0$ (with $i = 1 \dots, n$) and attached to point B_i on the object, with ${}^B\mathbf{b}_i \in \mathbb{R}^3$ representing the constant position of B_i expressed in \mathcal{F}_B ¹. Let $\mathbf{q}_i \in S^2$ be the configuration of the i^{th} cable in \mathcal{F}_W , T_i its tension, and

$$\mathbf{f}_i = T_i \mathbf{q}_i \quad (1)$$

be the coordinates in \mathcal{F}_W of the force that the i^{th} cable exerts on the load. The cables' mass and inertia are considered negligible compared to the robots' and object's ones, and cables are considered in tension under the effect of the weight [21], [14] (and so $T_i \neq 0$). Each cable is attached, at the other end, to a point on an aerial robot (flying carrier), whose position in \mathcal{F}_W is denoted with $\mathbf{p}_{Ri} \in \mathbb{R}^3$.

The dynamics of the transported object is described by

$$m_L \ddot{\mathbf{p}}_L = -m_L g \mathbf{e}_3 + \sum_{i=1}^n \mathbf{f}_i \quad (2)$$

$$\mathbf{J}_L {}^B \dot{\boldsymbol{\omega}}_L = -\mathbf{J}_L {}^B \boldsymbol{\omega}_L \times {}^B \boldsymbol{\omega}_L + \sum_{i=1}^n S({}^B \mathbf{b}_i) \mathbf{R}_L \mathbf{f}_i \quad (3)$$

$$\dot{\mathbf{R}}_L = S(\boldsymbol{\omega}_L) \mathbf{R}_L \quad (4)$$

where m_L, \mathbf{J}_L are the mass and the rotational inertia of the rigid body load and $S(\star)$ indicates the skew-symmetric operator implementing the cross product between two vectors.

The position and velocity of the i^{th} flying carrier in \mathcal{F}_W are, from the system's kinematics, equal to

$$\mathbf{p}_{Ri} = \mathbf{p}_L + \mathbf{R}_L {}^B \mathbf{b}_i + \mathbf{q}_i L_i \quad (5)$$

$$\dot{\mathbf{p}}_{Ri} = \dot{\mathbf{p}}_L + \dot{\mathbf{R}}_L {}^B \mathbf{b}_i + \dot{\mathbf{q}}_i L_i. \quad (6)$$

To compactly rewrite the load dynamics we use the matrix $\mathbf{G} \in \mathbb{R}^{6 \times 3n}$ that maps the cable forces to the wrench applied

at the object's center of mass, referred to as grasp matrix in the literature [22], [23]

$$\mathbf{G} = \begin{bmatrix} \mathbf{I}_3 & \mathbf{I}_3 & \dots & \mathbf{I}_3 \\ S({}^B \mathbf{b}_1) \mathbf{R}_L & S({}^B \mathbf{b}_2) \mathbf{R}_L & \dots & S({}^B \mathbf{b}_n) \mathbf{R}_L \end{bmatrix}. \quad (7)$$

The load dynamics (2)-(3) can be compactly rewritten as

$$\mathbf{W} = \mathbf{G} \mathbf{f} \quad (8)$$

where $\mathbf{f} = [\mathbf{f}_1^\top \ \mathbf{f}_2^\top \ \dots \ \mathbf{f}_n^\top]^\top$ stacks all forces that the cables apply to the object and $\mathbf{W} = \begin{bmatrix} m_L (\ddot{\mathbf{p}}_L + g \mathbf{e}_3) \\ \mathbf{J}_L {}^B \dot{\boldsymbol{\omega}}_L + \mathbf{J}_L {}^B \boldsymbol{\omega}_L \times {}^B \boldsymbol{\omega}_L \end{bmatrix}$.

Inverting (8), see [24], we obtain an expression for all the cable forces \mathbf{f} that are compatible with a certain \mathbf{W}

$$\mathbf{f} = \mathbf{G}^\dagger \mathbf{W} + \mathbf{N} \boldsymbol{\lambda}, \quad (9)$$

being \star^\dagger indicating the Moore-Penrose pseudo-inverse, $\mathbf{N} \in \mathbb{R}^{3n \times m}$ being the nullspace projector of the grasp matrix \mathbf{G} (with m the dimension of the nullspace of \mathbf{G}), and $\boldsymbol{\lambda} \in \mathbb{R}^m$ a column vector containing m free parameters $\lambda_1, \dots, \lambda_m$ referred to as the *internal forces* [22].

For each load forced equilibrium or trajectory defined by the load state and the corresponding forcing input \mathbf{W} we can obtain from (9) all the cable forces that are compatible with such load equilibrium/trajectory. These forces are parameterized by $\boldsymbol{\lambda}$. In turn, to each cable force corresponds a carrier position obtained by (5) substituting $\mathbf{q}_i = \mathbf{f}_i / T_i$, i.e., $\mathbf{q}_i = \mathbf{f}_i / \|\mathbf{f}_i\|$. So we can conclude that for any given load equilibrium/trajectory there are ∞^m compatible multi-UAV coordinated trajectories which are parameterized by the internal forces $\boldsymbol{\lambda}$ and are obtained by plugging (9) in (5).

B. Maintaining Load Static Equilibrium with non-stop flights

Internal forces have been exploited in the literature of cooperative aerial manipulation of suspended objects to, e.g., optimize the tension distribution in the carriers' cables [19], perform obstacle avoidance [25], or stabilize the object's pose in a force-based manipulation scenario [14]. However, all the aforementioned works consider multirotor UAVs that can stop (i.e., set $\dot{\mathbf{p}}_{Ri} = \mathbf{0}$) during the manipulation task execution.

Departing from the previous literature, in this work we explore whether the internal forces can be exploited to allow the flying carriers to keep loitering with $\|\dot{\mathbf{p}}_{Ri}\| \geq \underline{v} > 0$ while the load is kept to a static pose i.e., $\dot{\mathbf{p}}_L = {}^B \boldsymbol{\omega}_L = \mathbf{0}$.

Consider a static equilibrium of the suspended load characterized by position $\bar{\mathbf{p}}_L$ and orientation $\bar{\mathbf{R}}_L$. When the load is at static equilibrium, the only way the cable forces can still change is thanks to a change of the internal forces $\boldsymbol{\lambda}$ since they are the only time-varying parameters in (9) in that case. For analyzing the effect of changing internal forces we write them as the state of the following dynamical system:

$$\begin{cases} \dot{\boldsymbol{\lambda}} = \mathbf{u}_\lambda \\ \boldsymbol{\lambda}(0) = \boldsymbol{\lambda}_0 \end{cases}$$

where \mathbf{u}_λ acts as an input that we can assign and $\boldsymbol{\lambda}_0$ is their initial condition.

¹The left superscript, W if omitted, expresses the reference frame.

Problem 1 (pose regulation with non-stop flights). Assume that $\mathbf{p}_L(0) = \bar{\mathbf{p}}_L$ and $\mathbf{R}_L(0) = \bar{\mathbf{R}}_L$. We ask if there exists a n and a trajectory $\boldsymbol{\lambda}(t)$ such that $\forall t \geq 0$,

$$\begin{cases} \mathbf{p}_L(t) = \bar{\mathbf{p}}_L, \\ \mathbf{R}_L(t) = \bar{\mathbf{R}}_L, \\ \|\dot{\mathbf{p}}_{Ri}(t)\| \geq \underline{v} > 0, \quad \forall i = 1, \dots, n \\ -\infty < \underline{\lambda} \leq \lambda_i(t) \leq \bar{\lambda} < \infty, \quad \forall i = 1, \dots, n \end{cases} \quad (10)$$

The first two equations in (10) impose static equilibrium of the load. The third equation, where \underline{v} is a constant, is a lower bound to the norms of the flying carriers' velocities to impose that they do not stop while maintaining the desired constant pose of the object. Finally, the last expression in (10) imposes that each component of $\boldsymbol{\lambda}$ is bounded by certain upper and lower bounds, $\bar{\lambda}, \underline{\lambda}$. This last constraint has clear practical reasons as internal forces of too large magnitude in (9) generate cable forces that will eventually break the system.

When (10) holds, (9) can be rewritten component-wise as

$$\mathbf{f}_i(t) = \mathbf{f}_{0i} + \tilde{\mathbf{f}}_i(t), \quad (11)$$

where \mathbf{f}_{0i} is the component of each force that comes from the first term in the left-hand side (LHS) of (9), namely $\mathbf{G}^\dagger \mathbf{W}$; it balances the external wrench and is constant when the load is static. Instead, $\tilde{\mathbf{f}}_i$ is the variable component of the cable force generated by the internal forces, which comes from $N\boldsymbol{\lambda}(t)$ in (9).

Taking the time derivative of (9) we obtain:

$$\dot{\mathbf{f}} = N\dot{\boldsymbol{\lambda}}. \quad (12)$$

Equation (12) gives us a relationship between the internal force variation and the total cable force variation; to give an intuition, it gives all the possible variations of the cable forces, and hence of the carriers' velocities, that do not perturb the object pose equilibrium.

By differentiating (1) w.r.t. time, the cable force variation (12) it holds

$$\dot{\mathbf{f}}_i = \dot{T}_i \mathbf{q}_i + T_i \dot{\mathbf{q}}_i, \quad (13)$$

i.e., the force variation is composed of two orthogonal components: one is directed as \mathbf{q}_i (along the cable), and one as $\dot{\mathbf{q}}_i$ (orthogonal to the cable).

III. NON-STOP FLIGHT ANALYSIS

In this section, we will reply to the question: 'are non-stop carrier UAV flights compatible with keeping cable-suspended objects at a static pose?', which is formally stated in Problem 1.

First, we introduce here a few tools to reply to the above-formulated research question. We start by formalizing an intuitive condition.

Proposition 1. *When the load is at a static equilibrium and the cables are in tension,*

$$\exists \underline{v} > 0 \text{ s.t. } \forall t \|\dot{\mathbf{p}}_{Ri}(t)\| \geq \underline{v} \implies \exists s > 0 \text{ s.t. } \forall t \|\dot{\mathbf{f}}_i(t)\| \geq s$$

Proof. By computing (6) at the load's static equilibrium, we have

$$\dot{\mathbf{p}}_{Ri} = \dot{\mathbf{q}}_i L_i. \quad (14)$$

Hence, by using $\|\dot{\mathbf{p}}_{Ri}\| \geq \underline{v}$ inside (14) and given that the cable length L_i is greater than zero, we obtain

$$\|\dot{\mathbf{q}}_i\| \geq \frac{\underline{v}}{L_i}. \quad (15)$$

Consider now that, from (13), the cable forces vary along two orthogonal directions. That, plus the fact that \mathbf{q}_i is a unit vector by definition, leads to

$$\|\dot{\mathbf{f}}_i\| = |\dot{T}_i| + |T_i| \|\dot{\mathbf{q}}_i\| \quad (16)$$

Now, starting from (13) and using (15), (16), $L_i > 0$ and $|T_i| \neq 0$ by hypothesis of tensioned cables, we write:

$$\|\dot{\mathbf{f}}_i\| = |\dot{T}_i| + |T_i| \|\dot{\mathbf{q}}_i\| \geq |\dot{T}_i| + |T_i| \frac{\underline{v}}{L_i} \geq |T_i| \frac{\underline{v}}{L_i} := s > 0. \quad \square$$

Remark 1. Proposition 1 tells us that the lower boundedness of the norms of the cable forces derivatives is a necessary condition for (10) to hold. Namely, in reverse, if the norms of the cable forces derivatives are not lower bounded, then non-stop flights are impossible (i.e., $\nexists s > 0$ s.t. $\forall t \|\dot{\mathbf{f}}_i(t)\| \geq s \implies \nexists \underline{v} > 0$ s.t. $\forall t \|\dot{\mathbf{p}}_{Ri}\| \geq \underline{v}$).

A. 1-carrier case

First, we consider the case in which there is only one flying carrier, i.e., it is $n = 1$. The sole equilibrium points of the system are in this case the ones in which the load's center of mass lies below the vertical cable that suspends it².

The grasp matrix in (7) is

$$\mathbf{G} = \begin{bmatrix} \mathbf{I}_3 \\ S(\mathbf{B}\mathbf{b}_1)\mathbf{R}_L \end{bmatrix}.$$

Hence, as the grasp matrix $\mathbf{G} \in \mathbb{R}^{6 \times 3}$ has number of columns smaller than the number of rows, it has a trivial nullspace and $N = 0$.

Fact 1. *For $n = 1$, $\nexists t$ such that conditions (10) hold.*

Proof. $N = 0$ implies that (12) becomes $\dot{\mathbf{f}} \equiv \mathbf{0}$. According to (13), the cable force varies along two orthogonal components. Hence, the only way in which $\dot{\mathbf{f}}_i = \mathbf{0}$ is that both those orthogonal components are equal to zero. In other words, both $\dot{T}_i = 0$ and $\dot{\mathbf{q}}_i = \mathbf{0}$ (because $T_i \neq 0$ by assumption). When the load is at equilibrium, $\dot{\mathbf{p}}_L = \mathbf{0}$ and $\dot{\mathbf{R}}_L = \mathbf{0}$. By applying all the above conditions to (6), one obtains $\dot{\mathbf{p}}_{Ri} = \mathbf{0}$. \square

In conclusion, Fact 1 tells that for $n = 1$ non-stop flights for maintaining the static equilibrium of a suspended object are not possible.

²Despite this number of carrier(s) does not allow regulating the full pose of a suspended object, we are here interested in understanding if the carrier(s) can loiter while the object is at a static equilibrium.

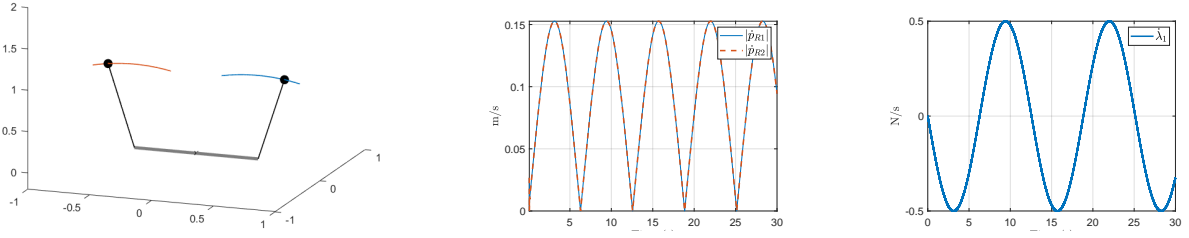


Fig. 4: On the left: two carriers (black dots) cannot maintain the pose of the object (in grey) while performing non-stop flights; the cables are in black, and colored curves are the carrier's paths. Carriers' velocities and $\dot{\lambda}$ are reported in the other two plots.

vectors $\mathbf{b}_{i,j}$ and $\mathbf{b}_{i,k}$ with $j, k \neq i$ and $j \neq k$, according to (18). From the hypotheses of the proposition, we have that \mathbf{f}_{0i} does not belong to P_i . Since \mathbf{f}_{0i} is constant and nonzero, also $\dot{\mathbf{f}}_i$ does not belong to P_i . On the other hand, from (12), we have that $\dot{\mathbf{f}}_i$ belongs to P_i . As a consequence, thanks also to the hypothesis that $\dot{\mathbf{f}}_i \neq \mathbf{0}$, we obtain that $\dot{\mathbf{f}}_i$ and \mathbf{f}_i are never parallel to each other (two parallel vectors must belong to the same plane). In other words, the angle between each cable force and its derivative is $0 < \angle(\mathbf{f}_i, \dot{\mathbf{f}}_i) < \pi$.

Because of the boundedness of each component of $\dot{\lambda}$, the endpoint of $\dot{\mathbf{f}}_i$ is constrained inside a bounded set denoted with $\tilde{P}_i \subset P_i$, the dark grey region in Figure 2. \tilde{P}_i is centered around the end-point of \mathbf{f}_{0i} and contains the vector $\dot{\mathbf{f}}_i$. For each \mathbf{f}_i , with $i = 1, 2, 3$, we have a minimum and maximum of the angle $\angle(\mathbf{f}_i, \dot{\mathbf{f}}_i)$ when $\dot{\mathbf{f}}_i$ varies in \tilde{P}_i , which we denote as $\underline{\alpha}(\mathbf{f}_i)$ and $\overline{\beta}(\mathbf{f}_i)$ respectively. We denote with $\underline{\alpha}$ and $\overline{\beta}$ the minimum and maximum of $\alpha(\mathbf{f}_i)$ and $\beta(\mathbf{f}_i)$ when the end point of \mathbf{f}_i varies in \tilde{P}_i , and i varies in $\{1, 2, 3\}$, respectively. Since those functions are continuous and the set \tilde{P}_i is bounded such minimum and maximum exist and therefore, for what has been previously said, they are such that $0 < \underline{\alpha} \leq \overline{\beta} < \pi$.

Now let's consider the two orthogonal components of $\dot{\mathbf{f}}_i$ defined in (13), i.e. $T_i \dot{\mathbf{q}}_i$ and $\hat{T}_i \dot{\mathbf{q}}_i$. These three vectors define a plane that contains also $\mathbf{f}_i = T_i \mathbf{q}_i$. We represent such a plane in Figure 3, where the bounds of the angles between $\dot{\mathbf{f}}_i$ and the direction of the force \mathbf{f}_i , given by \mathbf{q}_i , are represented by the dashed lines. Moreover, the lower bound of the norm of the force derivative, $s > 0$, is represented by a dotted circle; the endpoint of $\dot{\mathbf{f}}_i$ is constrained to be outside of that circle. Hence, its component on the direction orthogonal to the force, namely the one parallel to $\hat{\mathbf{q}}_i$, must lie in the green regions in Figure 3, delimited by the lines at distance $\underline{v}'' > 0$ from the line where \mathbf{f}_i lies. This gives a geometrical proof that $\|\hat{\mathbf{q}}_i\| T_i \geq \underline{v}''$ and so $\|\hat{\mathbf{q}}_i\| \geq \frac{\underline{v}''}{T_i} := \underline{v}' > 0$. \square

We are now ready to state the main result.

Fact 3. *If the load's static equilibrium is such that $\forall i \mathbf{f}_{0i} \notin \text{span}\{\mathbf{b}_{i,j}, \mathbf{b}_{i,k}\}$, with $i, j, k \in \{1, 2, 3\}$, $i \neq j \neq k \neq i$, then for $n = 3$ there exists infinite trajectories $\lambda(t)$ such that (10) is verified. A possible choice is to select $\forall i \in \{1, 2, 3\}$ the following sinusoidal functions*

$$\lambda_i(t) = \lambda_i(0) + A \cos(\psi t + \Phi_i) \quad (19)$$

where $\psi > 0$; the amplitude A is constant and bounded ($0 < A < \infty$); the initial condition is bounded $\underline{\lambda} \leq \lambda_i(0) \leq \overline{\lambda}$;

and the constant phases Φ_i are such that $0 < \Phi_i \leq \Phi_i \leq \overline{\Phi} < \pi$, and that, for every $j \neq i$ $|\Phi_i - \Phi_j| \geq \phi > 0$ (non-coinciding phases).

Proof. We are going to show that, choosing the aforementioned trajectories, $\|\dot{\mathbf{f}}_i\|$ is lower bounded, so we can apply Proposition 2. Let us consider without loss of generality the force applied by cable 1. From equation (12),

$$\dot{\mathbf{f}}_1 = \dot{\lambda}_1 \mathbf{b}_{1,2} + \dot{\lambda}_3 \mathbf{b}_{1,3}. \quad (20)$$

When λ_1 and λ_3 are chosen as in (19), they are bounded because the initial conditions and amplitudes A are bounded. Especially, $\forall t, |\lambda_i(t)| \leq |\lambda_i(0)| + |A|$. Moreover, their derivatives are $\dot{\lambda}_i = -A\psi \sin(\psi t + \Phi_i)$. Since $\mathbf{b}_{1,2}$ and $\mathbf{b}_{1,3}$ are not parallel, for $\|\dot{\mathbf{f}}_1\|$ to be lower bounded it is sufficient to show that at least one among $|\dot{\lambda}_1(t)|$ and $|\dot{\lambda}_3(t)|$ is non-zero at any time t , which is ensured by the non-coinciding phase assumption on Φ_1 and Φ_2 . \square

Remark: Fact 3 positively answer Problem 1 telling us that pose regulation of a suspended object using non-stop flying carriers is possible for $n = 3$.

D. Degenerate situations in the 3-carrier case

Even though we showed that it is possible for 3 flying carriers to maintain a constant pose of suspended objects without stopping, it is also interesting to analyze special choices of $\dot{\lambda}$, if any, that do not generate non-stop flights even for 3 carriers.

a) *3 carriers—degenerate case 1:* If two components of $\dot{\lambda}$, let us consider without loss of generality $\dot{\lambda}_1$ and $\dot{\lambda}_3$, are such that $\dot{\lambda}_3 = a \dot{\lambda}_1$, $a \in \mathbb{R}$, then the corresponding force variation, in this case as in (20), becomes

$$\dot{\mathbf{f}}_1(t) = (a + 1) \dot{\lambda}_1(t) (\mathbf{b}_{1,2} + \mathbf{b}_{1,3}), \quad (21)$$

which implies that $\dot{\mathbf{f}}_1$ lies along a constant direction over time, similar to what happens for the two-carrier case. In fact, since $\mathbf{b}_{1,2}$ and $\mathbf{b}_{1,3}$ are constant vectors this case resembles the two-carrier case displayed in (17). So, for the same reasoning of the proof of Fact 2, the velocity of carrier 1 is not lower bounded for all time, and so (10) does not hold.

b) *3 carriers—degenerate case 2:* In any case in which $\exists t : \dot{\lambda}_i(t) = \dot{\lambda}_j(t) = 0$ for some $i \neq j \in \{1, 2, 3\}$ then the corresponding force is zero at that time instant. For the same reasoning done in the proof of Fact 1, the corresponding carrier stops. Differently from the situation

(a) Three flying carriers execute non-stop flights not perturbing the pose of the suspended object.

(b) One of the carriers stops when two components $\dot{\lambda}_i$ are equal to each other.

(c) One of the carriers stops when the two components $\dot{\lambda}_i$ vanish simultaneously.

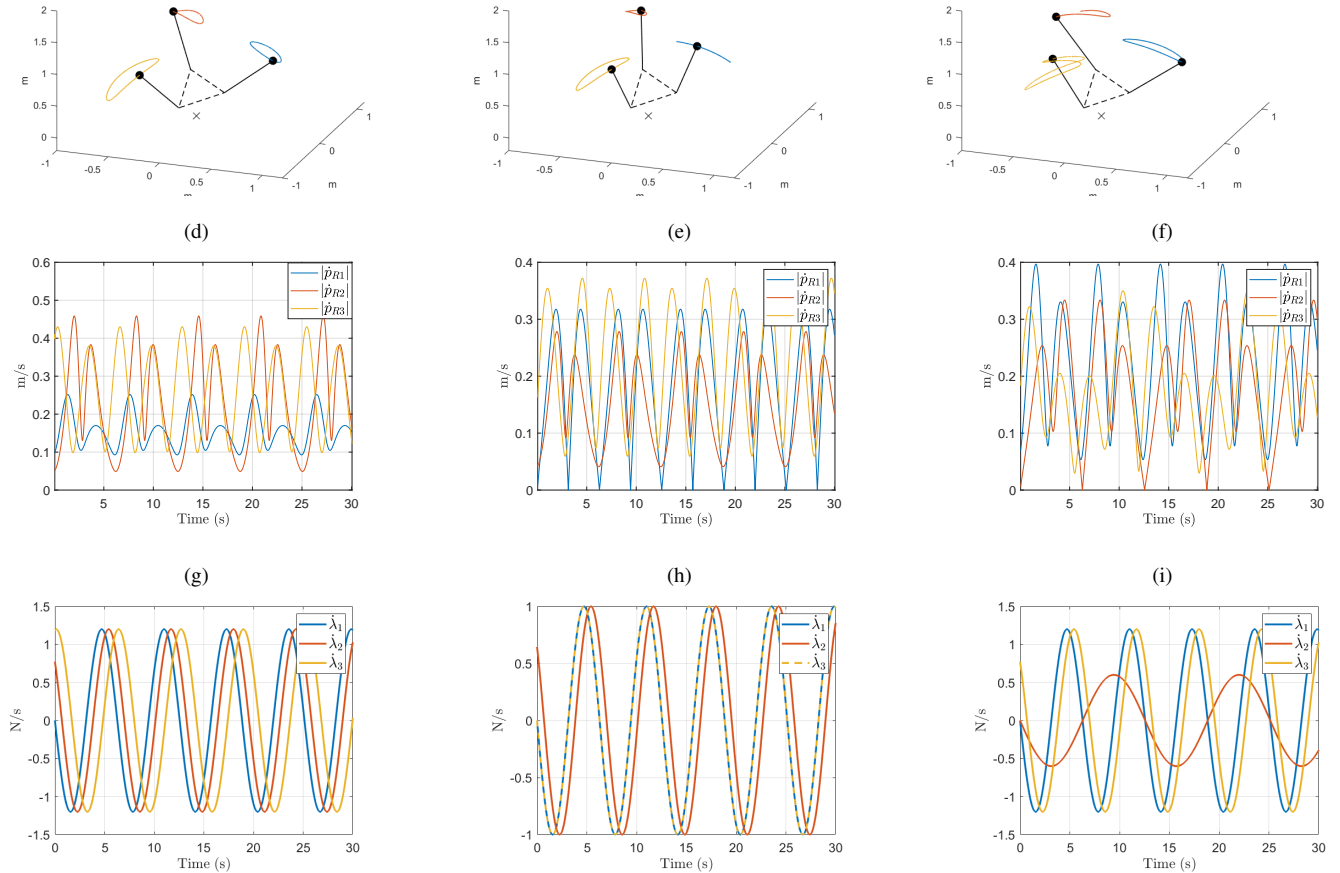


Fig. 5: Results of three different simulations, one in each column. On the leftmost column, non-stop flights are shown; in the other two columns, cases in which the carriers stop. On the first row of each simulation, a frame in which the 3 flying carriers (black dots) maintain the suspended object at a constant pose. Dotted lines connect the cables' attachment points on the object; the cables are black lines; the path of each carrier is a colored line (blue for carrier 1, red for carrier 2, and yellow for carrier 3); the cross is the object CoM. The values of $\|\dot{\mathbf{p}}_{Ri}\|$ and $\dot{\lambda}_i$ are also reported for each simulation.

described in case *a*), the cable force variation generally is not on a straight line.

IV. NUMERICAL RESULTS

In this section, we propose simulation results that support the previously presented results. A video of the simulation results can be found at <https://youtu.be/A18oq4oTQI8>. The simulations have been carried out in Matlab-Simulink. The dynamics of each carrier is a double integrator controlled through a PD feedback law to follow a desired trajectory. Indeed, the scope of this work is to assess the feasibility of non-stop flights for the considered application. The implementation considering more realistic non-stop UAV dynamics is left for future work.

The carriers' mass is 0.1 kg, and the derivative and proportional gain matrices are diagonal with values on the diagonals equal to 1.5 Ns/m and 1000 N/m, respectively.

The rigid body object is suspended below the cables, it has a mass equal to 1 kg and diagonal rotational inertia with

diagonal elements equal to 0.01 N·m/s.

Viscous friction on the load and cables' elasticity have been introduced in the simulator to test the theoretical results on more realistic conditions. Viscous friction on the translational and rotational dynamics is equal to 0.1 N·s/m and 0.1 rad·s/m is added to the object's dynamics to simulate friction with the air. The cables are massless linear springs with a rest length of 0.8 m and rigidity $K_c = 500 \frac{\text{N}}{\text{m}}$.

Each internal force is chosen as in (19), with parameters given in the following. The corresponding cable force variations are computed as in (12) and the carriers' trajectories from (5) and (6).

First, an example with 2 carriers is in Figure 4. The cable attachment points are such that $\mathbf{b}_{1,2} = \pm[0.5 \ 0 \ 0] \text{ m}$; $\lambda_1(0) = 1 \text{ N}$, $A_i = 1 \text{ N}$, $\psi_1 = 0.5 \text{ rad/s}$, $\Phi_1 = 0$. As predicted from the theory, the carriers stop during their motion when $\dot{\lambda}_1$ change sign, which is ultimately necessary to keep bounded cable forces.

Figure 5a shows frames in which 3 carriers manipulate the object with $\forall i, \lambda_i(0) = 2 \text{ N}$, $A = 1.2 \text{ N}$, $\psi = 2 \text{ rad/s}$, $\Phi_1 = 0$, $\Phi_2 = 0.7 \text{ rad}$, and $\Phi_3 = 1.7 \text{ rad}$. The cable attachment points for 3 carriers are such that $\mathbf{b}_1 = [0.259 \ 0.034 \ 0.399]^\top \text{ m}$, $\mathbf{b}_2 = [-0.156 \ 0.269 \ 0.556]^\top \text{ m}$, and $\mathbf{b}_3 = [-0.1223 \ -0.1399 \ 0.1778]^\top \text{ m}$. As all λ_i vary according to (20), at the same frequency and such that $\dot{\lambda}_i$ does not vanish simultaneously, the carriers follow non-stop elliptical-like paths on the sphere around their cable attachment point. The corresponding velocities of the carriers and $\dot{\lambda}$ are reported in Figures 5d and 5g, respectively, where it can be appreciated that the norm of the carrier velocities are always larger than a positive constant.

Figure 5b and 5c show what was referred to as degenerate cases 1 and 2, respectively: 3 carriers maintain the object's pose but one of them stops along the path. In the simulation of case 1, $\forall i, \lambda_i(0) = 2 \text{ N}$, $A = 1 \text{ N}$, $\psi = 1 \text{ rad/s}$, $\Phi_1 = \Phi_3 = 0$ and $\Phi_2 = 0.7 \text{ rad}$. In the simulation of case 2, instead, $\forall i, \lambda_i(0) = 2 \text{ N}$, $A = 1.2 \text{ N}$, $\psi_1 = \psi_3 = 1 \text{ rad/s}$, $\psi_2 = 0.5 \text{ rad/s}$, $\Phi_1 = \Phi_2 = 0$, and $\Phi_3 = 0.7 \text{ rad}$. As it can be seen in Figures 5h and 5i, for some time instants $\dot{\lambda}_1 = \dot{\lambda}_j = 0$. At the same time instants, the velocity of one carrier (in Figure 5e and 5f, respectively) goes to zero, too, as predicted by the theory.

V. CONCLUSIONS AND FUTURE WORK

This work studied the possibility of non-stop carrier flights while maintaining a constant pose of cable-suspended objects. After showing that non-stop flights are not feasible for only one or two flying carriers, we showed that three carriers can follow non-stop flights while maintaining the object's pose constant. We also highlighted degenerate cases in which non-stop flight is not achieved even for three carriers. Numerical examples supported the theoretical analysis.

In the future, we will extend the study to a generic number of carriers $n > 0$. We will design an optimal planning algorithm that generates smooth non-stop trajectories for UAVs, explicitly taking into account the system's constraints, such as the minimum forward speed of the robots, their maximum angular velocity, collision avoidance, etc. More realistic simulations will be implemented to assess the applicability of the method to VTOL hybrid platforms. Possible mechatronics adaptations to realize experiments will be considered.

REFERENCES

- [1] F. Ruggiero, V. Lippiello, and A. Ollero, "Aerial manipulation: A literature review," *IEEE Robotics and Automation Letters*, vol. 3, no. 3, pp. 1957–1964, 2018.
- [2] A. Ollero, M. Tognon, A. Suarez, D. Lee, and A. Franchi, "Past, present, and future of aerial robotic manipulators," *IEEE Transactions on Robotics*, vol. 38, no. 1, pp. 626–645, 2021.
- [3] J. Estevez, G. Garate, J. M. Lopez-Guede, and M. Larrea, "Review of aerial transportation of suspended-cable payloads with quadrotors," *Drones*, vol. 8, no. 2, 2024. [Online]. Available: <https://www.mdpi.com/2504-446X/8/2/35>
- [4] M. Bernard, K. Kondak, I. Maza, and A. Ollero, "Autonomous transportation and deployment with aerial robots for search and rescue missions," *Journal of Field Robotics*, vol. 28, no. 6, pp. 914–931, 2011.

- [5] N. Michael, J. Fink, and V. Kumar, "Cooperative manipulation and transportation with aerial robots," *Autonomous Robots*, vol. 30, pp. 73–86, 2011.
- [6] J. Fink, N. Michael, S. Kim, and V. Kumar, "Planning and control for cooperative manipulation and transportation with aerial robots," in *Robotics Research: The 14th International Symposium ISRR*. Springer, 2011, pp. 643–659.
- [7] G. Li, R. Ge, and G. Loianno, "Cooperative transportation of cable suspended payloads with mavs using monocular vision and inertial sensing," *IEEE Robotics and Automation Letters*, vol. 6, no. 3, pp. 5316–5323, 2021.
- [8] M. Gassner, T. Cieslewski, and D. Scaramuzza, "Dynamic collaboration without communication: Vision-based cable-suspended load transport with two quadrotors," in *2017 IEEE International Conference on Robotics and Automation (ICRA)*. IEEE, 2017, pp. 5196–5202.
- [9] K. Wahba and W. Hönig, "Efficient optimization-based cable force allocation for geometric control of a multirotor team transporting a payload," *IEEE Robotics and Automation Letters*, 2024.
- [10] J. Goodman and L. Colombo, "Geometric control of two quadrotors carrying a rigid rod with elastic cables," *Journal of Nonlinear Science*, vol. 32, no. 5, p. 65, 2022.
- [11] K. Sreenath, N. Michael, and V. Kumar, "Trajectory generation and control of a quadrotor with a cable-suspended load—a differentially-flat hybrid system," in *2013 IEEE international conference on robotics and automation*. IEEE, 2013, pp. 4888–4895.
- [12] P. O. Pereira, M. Herzog, and D. V. Dimarogonas, "Slung load transportation with a single aerial vehicle and disturbance removal," in *2016 24th Mediterranean conference on control and automation (MED)*. IEEE, 2016, pp. 671–676.
- [13] M. Bernard and K. Kondak, "Generic slung load transportation system using small size helicopters," in *2009 IEEE International Conference on Robotics and Automation*. IEEE, 2009, pp. 3258–3264.
- [14] C. Gabellieri, M. Tognon, D. Sanalitra, and A. Franchi, "Equilibria, stability, and sensitivity for the aerial suspended beam robotic system subject to parameter uncertainty," *IEEE Transactions on Robotics*, 2023.
- [15] P. O. Pereira, P. Roque, and D. V. Dimarogonas, "Asymmetric collaborative bar stabilization tethered to two heterogeneous aerial vehicles," in *2018 IEEE International Conference on Robotics and Automation (ICRA)*. IEEE, 2018, pp. 5247–5253.
- [16] T. Chen and J. Shan, "Cooperative transportation of cable-suspended slender payload using two quadrotors," in *2019 IEEE International Conference on Unmanned Systems (ICUS)*, 2019, pp. 432–437.
- [17] Q. Jiang and V. Kumar, "The inverse kinematics of cooperative transport with multiple aerial robots," *IEEE Transactions on Robotics*, vol. 29, no. 1, pp. 136–145, 2012.
- [18] K. Mohammadi, S. Sirouspour, and A. Grivani, "Passivity-based control of multiple quadrotors carrying a cable-suspended payload," *IEEE/ASME Transactions on Mechatronics*, vol. 27, no. 4, pp. 2390–2400, 2022.
- [19] C. Masone, H. H. Bühlhoff, and P. Stegagno, "Cooperative transportation of a payload using quadrotors: A reconfigurable cable-driven parallel robot," in *2016 IEEE/RSJ International Conference on Intelligent Robots and Systems (IROS)*, 2016, pp. 1623–1630.
- [20] S. Leutenegger, C. Hürzeler, A. K. Stowers, K. Alexis, M. W. Achtelik, D. Lentink, P. Y. Oh, and R. Siegwart, "Flying robots," *Springer Handbook of Robotics*, pp. 623–670, 2016.
- [21] D. Sanalitra, H. J. Savino, M. Tognon, J. Cortés, and A. Franchi, "Full-pose manipulation control of a cable-suspended load with multiple uavs under uncertainties," *IEEE Robotics and Automation Letters*, vol. 5, no. 2, pp. 2185–2191, 2020.
- [22] T. Yoshikawa, "Virtual truss model for characterization of internal forces for multiple finger grasps," *IEEE Transactions on Robotics and Automation*, vol. 15, no. 5, pp. 941–947, 1999.
- [23] M. Tognon, C. Gabellieri, L. Pallottino, and A. Franchi, "Aerial co-manipulation with cables: The role of internal force for equilibria, stability, and passivity," *IEEE Robotics and Automation Letters*, vol. 3, no. 3, pp. 2577–2583, 2018.
- [24] K. Sreenath and V. Kumar, "Dynamics, control and planning for cooperative manipulation of payloads suspended by cables from multiple quadrotor robots," *m*, vol. 1, no. r2, p. r3, 2013.
- [25] G. Li, X. Liu, and G. Loianno, "Safety-aware human-robot collaborative transportation and manipulation with multiple mavs," *arXiv preprint arXiv:2210.05894*, 2022.